UNIVERSITY *of*York

This is a repository copy of *Edge Computing Based Fault Sensing of the Distribution Cables Based on Time-domain Analysis of Grounding Line Current Signals*.

White Rose
university consortium
Universities of Leeds, Sheffield & York

Edge Computing Based Fault Sensing of the Distribution Cables Based on Time-domain Analysis of Grounding Line Current Signals

Nan Peng, *Associate Member*, *IEEE*, Xinyu Liu, Rui Liang, *Member*, *IEEE*, Zehua Tang, Xiaofeng Ren, Yihua Hu, *Senior Member*, *IEEE*, Guoxin Li

Abstract—Due to the complex structures and fault conditions, accurate fault sensing of the underground distribution cables is a difficult task. The distribution automation system (DAS) and fault indicator system (FIS) are only applicable to the severe faults. In addition, the current DAS and FIS are all based on the centralized data processing system (CDS), increasing the communication pressure and data processing time of the main station. Considering the advantages of edge computing, this paper investigates using the grounding line currents to sense the fault in distribution cable networks. First, an edge computing based fault sensing system (ECS) is designed. The equivalent time-domain distribution cable models considering multi-conductor mutual couplings are then established in both normal and fault cases. The time-domain features of the cable grounding line currents prior to and after the fault are analyzed to create the fault detection criterion. Combining the network topology, locations of the measurement units (MUs), and direction factor of the ground line current, a space matrix based algorithm is created to achieve fault cable section location at edge. Finally, a distribution cable network is created by PSCAD/EMTDC. Various simulations are conducted to validate the effectiveness and robustness of the algorithm.

Index Terms— distribution cables, grounding line current, fault sensing, edge computing

I. INTRODUCTION

POWER distribution networks, directly connected to the users, are located at the ends of power systems. The power supply reliability and quality are dependent on the distribution network which is both the basis and destination of the smart grid. With the expansion of the modern cities, the load density grows dramatically, which poses great challenges to the power supply reliability and safety.

The power distribution lines in the urban cities have been dominated by the underground cables due to the advantages of less land demand and effect on the city appearance [1]. For example, more than 95% of the over-head transmission lines have been replaced by the unground cables in the downtown of the large cities like Beijing and Shanghai in China. However, the power distribution cables are generally buried into the ground, laid in the cable trenches, or even soaked in the water, making an adverse working and monitoring condition.

Most of the cable faults result from insulation deterioration. The factors causing cable insulation deterioration include the external forces, environmental contamination, internal defects, etc. After long-time operation of the cable with an insulation defect, the partial discharge occurs at early stage. The insulation is then continuously damaged until totally breakdown, which produces the cable fault. According to the statistics, most of the faults in the distribution networks are the single-phase faults [2]. To avoid that the single-phase faults develop into more severe ones (like phase-to-phase circuit faults), it is necessary to detect them correctly and quickly. Fast and reliable cable fault sensing is conducive to expediting system restoration and reducing the power outage time [3]. However, after a single-phase fault occurs in the distribution network, the fault features are not obvious since the neutral of the whole system is commonly ineffectively grounded [4-5]. The complex condition of the fault and bad working environment add to the difficulty of sensing the faults in distribution cables.

Fault sensing of the distribution cables can be divided into two steps: fault detection and fault section location. The fault detection algorithms, mainly based on the abrupt changes in the voltage and current signals, are used to determine whether a fault occurs in the cable. To accelerate fault isolation, the fault section location algorithms are employed to locate the fault line after the fault is detected.

When a fault occurs in the distribution line, the voltages and currents deviate from the normal ones, providing the basis for sensing the fault. Different algorithms are adopted for fault detection in the distribution network and effective results are obtained. The algorithm in [6] detects the fault by using the neutral voltage displacement. The algorithm in [7] is based on estimating the zero-sequence capacitance to realize directional detection of phase-to-ground faults in the distribution network. The voltage harmonic distortion is employed to detect the fault

Nan Peng, Xinyu Liu, Zehua Tang and Guoxin Li are with the School of Electrical Engineering, China University of Mining and Technology, Xuzhou 221116, China (e-mail: pncumt@163.com, 17175325@cumt.edu.cn, zehua_tang@cumt.edu.cn, and guoxinlicumt@126.com).

Rui Liang is with the School of Electrical Engineering, China University of Mining and Technology, Xuzhou 221116, and the school of Automation, Huaiyin Institute of Technology, Huaian 223003, China (email: liangrui@cumt.edu.cn).

Xiaofeng Ren is with State Grid Xuzhou Power Supply Company, Xuzhou 221005, China (email: rxf_001@sina.com).

Yihua Hu is with Department of Electronic Engineering, University of York, Heslington, York, YO10 5DD, UK (email: yihua.hu@york.ac.uk).

Color versions of one or more of the figures in this paper are available online at http://ieeexplore.ieee.org.

Digital Object Identifier xxxxxx.

in [8]. The algorithm in [9] detects the cable fault by calculating the degree of change of the sheath current.

According to the types of the extracted fault features, the algorithms for fault section location generally fall into two main categories: the steady-state and transient-state algorithms [10]. The steady-state algorithms commonly use the amplitudes and phases of the voltages and currents to determine the fault section. By using the phase and amplitude of the voltage measured at the local bus, the voltage deviation of each candidate line is calculated to locate the fault section in [11]. The algorithm in [12] employs the voltage amplitude and phase variations at each bus node prior to and after the fault to construct a data bank to identify the fault section. Although the steady-state algorithms are easily implemented with low cost [13], they are susceptible to the complex fault conditions and system parameters.

After a fault occurs in the distribution network, the fault-generated transients contain rich information related to the fault location [14]. The transient-state algorithms, widely adopted in practice, are robust to the fault conditions and independent from system parameters. The transient voltage difference [15], voltage or current energy [16], and zero-sequence current [17] are used to identify the fault section. According to the distribution characteristics of zero-sequence currents and voltages, a fault section location criterion is proposed in [18] by defining the zero-sequence power in time-domain. In [19], the transient zero-sequence currents in the selected frequency band are acquired to locate the fault section. Based on the defined wavelet energy spectrum entropy, four different back-propagation artificial neural networks are built in [20] for determining the fault section.

As the most commonly used transient-state algorithms, the traveling wave-based algorithms have been widely used in transmission networks [21]. The fault section location algorithms based on traveling waves are also applied to the distribution networks. The algorithm in [22] extracts the arrival time of fault initial traveling wave and locates the fault section by the proposed fault branch determination matrix. Combined with the graph theory, the arrival time difference between the zero-mode and aerial-mode traveling waves is employed in [23] to construct the criterion for locating the fault section. Due to the high requirements for signal sampling, the implementation of the traveling wave algorithms is expensive. Additionally, the reflection and refraction of the traveling waves in the distribution network are complex, which limits the application of these algorithms [24].

To realize automatic fault sensing in field, many types of the intelligent measurement devices, such as the fault indicators [25], feeder terminal units [26], and μPMUs [27], have been mounted in the distribution networks. Considering the state information of the fault indicators, a fault section location algorithm is presented in [28] based on the network topology features. Based on the fuzzy Petri net, a fault section location algorithm is proposed in [29] by using the multi-source information of the smart meters. The current intelligent measurement devices are only applicable to the severe faults, such as the metallic grounding or short-circuit faults. They

cannot locate the complex single-phase faults such as the single-phase arcs.

In general, the algorithms for sensing the severe faults in the distribution networks with the overhead lines have shown good performance. However, the fault sensing of underground distribution cables has not been fully developed. First, the model of the three-core distribution cable is complicated due to its complex structure, and the electromagnetic coupling between the multiple conductors is more significant. Second, the three-phase core-conductors are wrapped by the insulating rubber, some types of the MUs cannot be installed along the cable. Third, the fault conditions in the distribution cables are more complex. The single-phase arc faults may occur in the cables, leading to the signal distortion.

In addition, the current fault sensing systems are based on the CDS at the main station. A large quantity of the measured data brings about significant communication pressure and computational burden to the main station, resulting in the low efficiency and reliability of fault sensing. With the proposal of the ubiquitous power internet of things and the development of related technologies, higher requirements are put forward for fault sensing of the distribution networks. Edge computing has the advantages of low end-to-end latency, low backbone network bandwidth consumption, both center and edge scalability, and lower risk for enroute attacks [30]. It connects the remote network to realize data sharing and collaboration [31-32]. To reduce the communication pressure of the main substation and minimize the response time, edge computing can be employed in the process of fault sensing of the distribution cables.

The distribution three-core cable sheaths are commonly grounded at both ends through the grounding lines to reduce the bad effect of the induced electromotive force. Compared with three-phase or zero-sequence currents, the grounding line currents are more easily acquired by the existing MUs in filed. Aiming at the distribution cable network, this paper constructs the time-domain model for the typical three-core cable to analyze the features of the grounding line currents prior to and after the fault. Based on the amplitude and directional features of the grounding line currents in the network, a simple and practical algorithm for sensing the fault is proposed and verified to be effective in various fault conditions. The main contributions are as follows:

(1) A lump-parameter equivalent circuit model in time domain composed of the impedances and admittances of the core-conductors and metallic sheath of the typical 10kV three-core distribution cable is constructed in the normal and fault conditions.

(2) The features of the direction factors and amplitudes of the grounding line currents are obtained in the time domain based on the rigorous theoretical analysis of the created model of the distribution cable.

(3) The proposed algorithm is verified to be applicable to different fault conditions including the arc faults by various fault simulations. Compared with the current algorithms, the proposed one has the advantages of convenient measurement, significant feature, no need for strict synchronization, low

sampling rate.

II. Edge Computing Based Fault Sensing

After a fault occurs in the distribution cable network, a smart fault sensing system with repaid response, high efficiency and reliability is expected to detect the fault and locate the fault cable. For the current CDS adopted in the actual field, a large amount of data is directly transmitted to the main station in the process of fault sensing. The whole process of fault sensing is undertaken by the main station. However, due to the limited communication bandwidth and computing resource, the station has been under long-term communication pressure and computational burden, resulting in a slow response of the station and low efficiency of fault sensing. Additionally, the fault sensing fails once the station is attacked, thus the fault sensing reliability of the CDS cannot be ensured.

To address the above problems of the CDS, the ECS is employed in fault sensing of the distribution cables. The architecture of the ECS is illustrated in Fig.1. In the figure, S and R represent the substation and ring network cabinet. The ECS consists of two layers: the device and the edge layers. In the device layer, the MUs and edge nodes are deployed in the cable branch boxes and feeder cabinets at the main bus. The grounding line currents at the local ends of the cables required for fault sensing are firstly captured by the MUs. The acquired current signals are then transmitted to the edge nodes in the edge layer by 4G or 5G [33]. In the edge layer, the edge nodes, capable of data processing and communication, firstly receive the data from the device layer. At the edge nodes, whether a fault occurs in the distribution cable is then determined. After a fault is detected, the fault cable is quickly located to achieve the fault warning. It can be observed that the fault sensing of the ECS is completely conducted at the edge nodes instead of the main station.
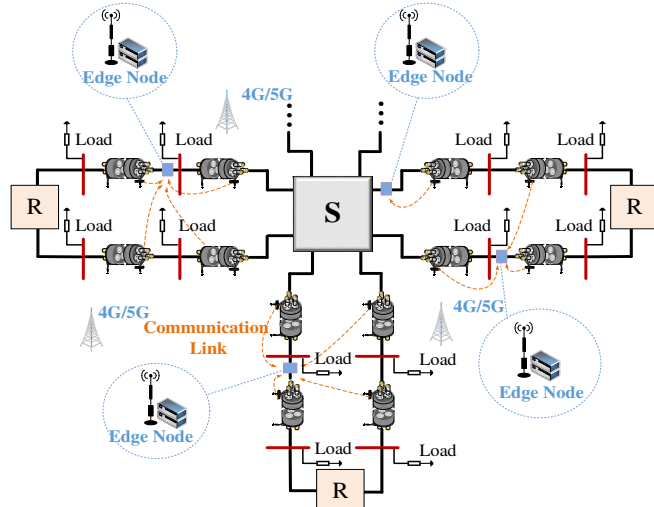

Fig.1 Architecture of the designed ECS.

Compared with the current CDS, the advantages of the ECS are explained in detail as follows. First, the communication pressure of the main station and fault sensing time can be greatly reduced by the ECS. The time of fault sensing by CDS and ECS t_{CDS} and t_{ECS} can be estimated by

$$\begin{cases} t_{\text{CDS}} = \dfrac{S_{d-DAS}}{v_1}, S_{d-DAS} = \dfrac{q_m \cdot S_f}{C_f - 1} \\ t_{\text{ECS}} = \dfrac{S_{d-FSS}}{v_2}, S_{d-FSS} = \dfrac{S_d}{N_{EC}} \end{cases} \quad (1)$$

where S_{d-DAS} and S_{d-FSS} represent the sizes of the data transmitted to the main station and the edge node. S_f is the size of the data recorded by a MU. v_1 and v_2 are the average data transmission rates in CDS and ECS. S_f contains C_f columns of data. q_m and N_{EC} denote the total numbers of the MUs and edge nodes in the distribution network. In the ECS, no data is transmitted to the main station, and the size of the data transmitted to each edge node is smaller than that transmitted to the main station in the CDS. For the same data transmission bandwidth, it is obvious that the average data transmission rate in the ECS is higher than that in the CDS. Thus, t_{CDS} is larger than t_{ECS}.

Second, the reliability of the whole data processing system can be significantly improved by the ECS. In the CDS, the fault sensing fails once the main station is attacked. However, since there is more than one edge node in the ECS and the data processing and computing are all completed by the edge nodes, the fault sensing continues as normal even if the main station or an edge node is attacked. In this case, the task of fault sensing will be accomplished by the remaining edge nodes.

A. Model of the Distribution Cable

The cross-section of a typical distribution cable is depicted in Fig.2. It can be seen that the three-phase conductors together with their sheaths are all arranged in an equilateral triangle. Since the structures are symmetrical, the three-core cables have the symmetric electrical parameters described by [34]

$$\begin{cases} Z_{AA} = Z_{BB} = Z_{CC} \\ Z_{AB} = Z_{BC} = Z_{CA} \\ Z_{AS} = Z_{BS} = Z_{CS} \doteq Z_{SS} \end{cases} \quad (2)$$

where Z_{PP} represents the self-impedance of the core conductor of phase P ($P \in \{A, B, C\}$) in per unit length of the cable. Z_{SS} denotes the self-impedance of the metallic sheath in per unit length of the cable. Z_{PQ} represents the mutual impedance between the core conductors of phases P and Q ($Q \in \{A, B, C\}$) in per unit length of the cable. Z_{PS} represents the mutual impedance between the core conductor of phase P and metallic sheath in per unit length of the cable. According to the structure and parameter of the cable, the equivalent electrical model of the distribution cable is shown in Appendix A.
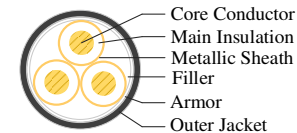

Fig.2 Diagram of the cross-section of the typical distribution cable.

For the typical three-core cable, the zero-sequence current transformers cannot be directly installed along the insulating rubber of the cable. They are commonly installed in the switchgear or the ring network cabinet. To install the transformers, the main insulation and metallic sheath are

stripped at the terminal of the cable to expose the core conductor. As shown in Fig.3, the zero-sequence current transformer is toroidal or rectangular, with a window which is large enough to enclose all three phase core conductors, adding to the difficulty of installation and dismantlement. Compared with the zero-sequence current, the grounding line current can be easily acquired at every cable section since the cable is generally grounded in section. The window of the transformer for measuring grounding line currents is relatively small, which is conducive to installation and dismantlement.
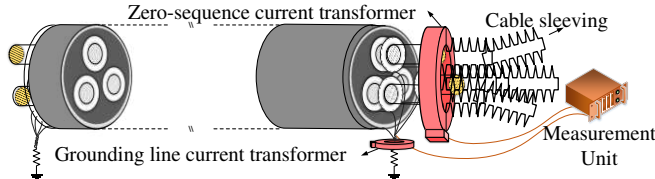

Fig.3 Comparison between the transformers for measuring the zero-sequence current and grounding line current.

B. Fault Sensing Algorithm

The process of the fault sensing consists of two stages: determine whether a fault occurs (cable fault detection) and where the fault occurs (fault cable location). In this subsection, the circuit analysis of the electrical model of the distribution cable in Appendix A is conducted to develop the cable fault detection and fault cable location criteria, which form a novel fault sensing algorithm.

A typical distribution cable network is displayed in Fig.4. Based on the models shown in Appendix, the theoretical analysis on the grounding line currents in both normal and fault conditions is conducted. Details are as follows.
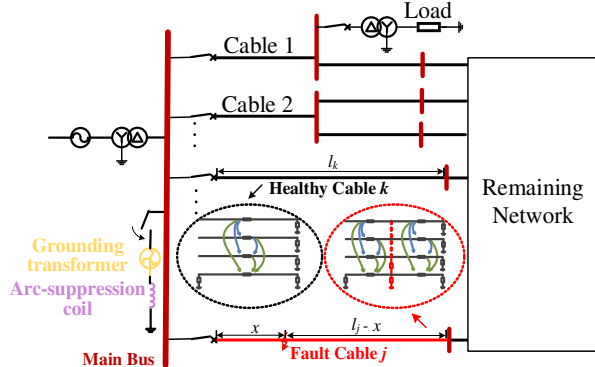

Fig.4 Diagram of a typical distribution cable network.

In normal operation, the relationship between the grounding line currents at both terminals of the three-core cable can be described by

$$\begin{cases} i_{LS}(t) = -i_{RS}(t), R_{SG}i_{LS}(t) = u_{SS}(t) + R_{SG}i_{RS}(t) \\ u_{SS}(t) = l\left[R_{AS}\left(i_{tol}(t) + i_{RS}(t)\right) + L_{AS}\frac{d\left(i_{tol}(t) + i_{RS}(t)\right)}{dt}\right] \\ i_{tol}(t) = i_{LA}(t) + i_{LB}(t) + i_{LC}(t) \doteq 0 \end{cases}(3)$$

where $i_{LS}(t)$ and $i_{RS}(t)$ are the grounding line currents at the local and remote ends of the cable. R_{AS} and L_{AS} represent the mutual resistance and inductance between phases A and sheath in per unit length of the three-core cable. $u_{SS}(t)$ is the voltage across $l \cdot Z_{SS}$ of the three-core cable before the fault. $i_{tol}(t)$ is the sum of the three-phase currents of the cable prior to the fault.

$i_{LA}(t)$, $i_{LB}(t)$, and $i_{LC}(t)$ are the currents in phases A, B, and C at the local end of the cable.

By solving (3), the grounding line current at the local end of the three-core cable in normal operation is formulated by

$$\begin{cases} i_{LS}(t) = e^{-\alpha t} \\ \alpha = \dfrac{2R_{SG} + l \cdot R_{AS}}{l \cdot L_{AS}} \end{cases}(4)$$

It can be seen from (4) that the grounding line currents at both terminals of the three-core cable are close to zero in normal operation. Thus, the cable fault can be detected by

$$\max_{t \geq t_0 + T}\left(\left| i_{LS}(t)\right|\right) > i_{LSM} \tag{5}$$

where t_0 is the time corresponding to the singularity point of $i_{LS}(t)$ induced by the fault. t_0 can be easily determined by the signal singularity detection algorithms [35]. T represents the time interval corresponding to the power frequency. i_{LSM} is the maximum grounding line current at the local end of the cable in normal operation. Since the waveform of the grounding line current signal prior to and after the fault can be recorded by the MU, i_{LSM} is set as the maximum value of the measured grounding line current prior to the fault. In simulation, the maximum value of the grounding line current before the fault occurs is only 0.01A which is less than the minimum range of the current MU. The minimum range of the MU in actual field is 0.1A. Thus, i_{LSM} is set as 0.1A.

When a fault occurs in cable j (shown in Fig.4), based on the model shown in Fig.A1, the grounding line current at the local end of any healthy cable k is constrained by

$$\begin{cases} h_k i_{ks}(t) + g_k \dfrac{di_{ks}(t)}{dt} = n_k i_{0k}(t) + w_k \dfrac{di_{0k}(t)}{dt}, t \geq t_0 \\ h_k = 2R_{SG} + l_k R_{PS}, g_k = l_k L_{PS}, n_k = 3l_k R_{PS}, w_k = 3l_k L_{PS} \end{cases}(6)$$

In (6), l_k is the length of cable k. $i_{ks}(t)$ represents the grounding line current at the local end of cable k after the fault. $i_{0k}(t)$ denotes the zero-mode current at the local end of cable k after the fault. R_{PS} and L_{PS} are the real and imaginary parts of Z_{PS}.

Similarly, by circuit analysis on the model shown in Fig.A2, we also have

$$\begin{cases} h_j i_{js}(t) + g_j \dfrac{d_{js}(t)}{dt} = n_j i_{0j}(t) + w_j \dfrac{di_{0j}(t)}{dt}, t \geq t_0 \\ h_j = R_{SG} - xR_{PS}, g_j = -xL_{PS}, n_j = xR_{PS}, w_j = xL_{PS} \end{cases}(7)$$

where $i_{js}(t)$ represents the grounding line current at the local end of the fault cable j. $i_{0j}(t)$ denotes the zero-mode current at the local end of cable j after the fault.

Based on (6)-(7), the amplitude of the grounding line current at the local end of the cable is verified to be larger than that of the zero-sequence current in theory. The details are shown in the Appendix B. Fig.5 displays the grounding line currents and zero-sequence currents of the healthy and fault cables in the same fault condition. $i_{0h}(t)$ and $i_{sh}(t)$ represent the zero-sequence and grounding line currents at the local end of the healthy cable. $i_{0f}(t)$ and $i_{sf}(t)$ denote the zero-sequence and grounding line currents at the local end of the fault cable. It can be seen that the fault feature of the grounding line current is more significant than that of the zero-sequence current. In general, it is more feasible and advantageous to use the

grounding line current for sensing the fault in the distribution cable.

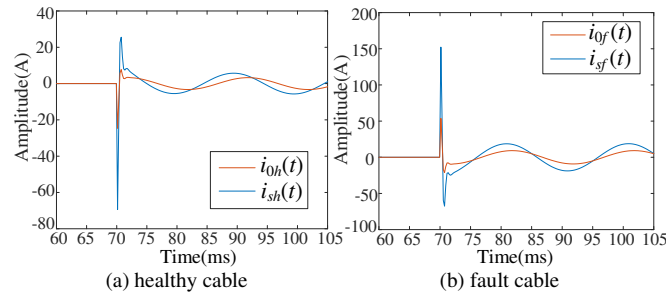(a) healthy cable   (b) fault cable

Fig.5 The grounding line currents and the zero-sequence ones at the local ends of the healthy and fault cables.

The distribution characteristics of the zero-mode currents of the cables connected to the main bus are given by

$$\begin{cases} i_{0j}(t) = -\sum_{\substack{k=1 \\ k \neq j}}^{M} i_{0k}(t) + i_{NS}(t,\omega), t \geq t_0 \\ i_{NS}(t,\omega) = \begin{cases} 0 & , \text{ungrounded} \\ i_{ARSUP}(t) \propto \dfrac{1}{\omega} & , \text{arc-suppression coil grounded} \end{cases} \end{cases} \quad (8)$$

where M is the total number of the cable feeders connected to the main bus. $i_{NS}(t,\omega)$ is the compensated current determined by the neutral grounding mode of the distribution network. $i_{ARSUP}(t)$ is the current induced by the arc-suppression coil. ω ($\omega > 0$) represents the signal angular frequency.

In an ungrounded distribution network, it is obvious that $i_{NS}(t,\omega) = 0$. In this case, considering (7) and (8), the relationship between the grounding line current and zero-mode current at the local end of cable j can be reformulated as

$$h_j i_{js}(t) + g_j \frac{d i_{js}(t)}{dt} = -\left(n_j \sum_{\substack{k=1 \\ k \neq j}}^{M} i_{0k\_af}(t) + w_j \frac{d\sum_{\substack{k=1 \\ k \neq j}}^{M} i_{0k\_af}(t)}{dt} \right), (t \geq t_0, \omega > 0) \quad (9)$$

By comparing (6) and (9), it can be concluded that direction of the grounding line current at the local end of the fault cable is opposite to that of any healthy cable.

According to (7) and (8), the grounding line current at the local end of cable j in an arc-suppression coil grounded distribution cable network is

$$h_j i_{js}(t) + g_j \frac{d i_{js}(t)}{dt} = -\left(\begin{array}{l} n_j \sum_{\substack{k=1 \\ k \neq j}}^{M} i_{0k}(t) + w_j \dfrac{d\sum_{\substack{k=1 \\ k \neq j}}^{M} i_{0k}(t)}{dt} + \\ n_j i_{ARSUP}(t,\omega) + w_j \dfrac{d i_{ARSUP}(t,\omega)}{dt} \end{array} \right) \quad (10)$$

Since $i_{ARSUP}(t,\omega)$ is inversely proportional to ω, there must exist a cut-off frequency ω_c which makes $i_{ARSUP}(t,\omega) \approx 0$ when $\omega > \omega_c$. In this case, we have

$$h_j i_{js}(t) + g_j \frac{d i_{js}(t)}{dt} = -\left(n_j \sum_{\substack{k=1 \\ k \neq j}}^{M} i_{0k}(t) + w_j \frac{d\sum_{\substack{k=1 \\ k \neq j}}^{M} i_{0k}(t)}{dt} \right), (t \geq t_0, \omega > \omega_c) \quad (11)$$

Based on the above analysis, the relationship between the directions of the grounding line currents of the fault cable j and any healthy cable k can be shown by

$$D_j = -D_k, \quad (k \in \{1,2,...,M\} \ \& \ k \neq j) \quad (12)$$

where D_j and D_k represent the direction factors of the grounding line currents of cable j and k. The sign of D_j (or D_k) reflects the direction of the grounding line current of cable j (or k). The relationship in (12) holds true with $\omega > 0$ and $\omega > \omega_c$ for the ungrounded and arc-suppression coil grounded distribution cable networks. Taking the grounding line current of the any cable (cable 1) as a reference, the direction factor D_k of the grounding line current of any other cable k can be quickly determined by

$$\begin{cases} D_k = 1 & , k = 1 \\ D_k = sign\left(\displaystyle\sum_{\substack{a=a_0 \\ a \in Z_+}}^{\Delta t \times f_S} sign\left(i_{1s}(a) \times i_{ks}(a) \right) \right), & k > 1 \end{cases} \quad (13)$$

where $sign(\ )$ represents the sign function. a is the sampling point variable. a_0 denotes the sampling point corresponding to t_0. f_S is the sampling rate.

There are many cable branches in the actual distribution cable networks. Although the fault section can be determined by applying (12) to each branch node, the fault section location in this way will be slow and laborious. To efficiently and automatically detect the fault section, a space matrix based algorithm, considering the network topology and measurement locations, is proposed as shown below.

The space matrix M_S of any cable feeder is defined as $M_S=[m_{iy}]_{p \times q}$. p and q represent the numbers of the nodes and MUs of the cable feeder, respectively. m_{iy} is the element in the ith ($1 \leq i \leq p$) row and yth ($1 \leq y \leq q$) column of M_S. The row and column of M_S correspond to the node and MU. If MU y lies in the local end of the cable between nodes i and $i+1$, the elements m_{iy} and $m_{(i+1)y}$ are set as 1 and the remaining elements in column y are equal to 0. The distance vector V_D of the cable feeder is defined as $V_D=[v_i]_{p \times 1}$ where v_i represents the ith element (corresponding to node i) in V_D. v_i is the total length of the cables between the local end of the cable feeder and node i. $D_m=[D_y]_{1 \times q}$ is the vector of the direction factor. D_y denotes the yth element (corresponding to the direction of the grounding line current captured by MU y). D_y can be computed by (13). D_m and V_D contain the information on the measurements and nodes corresponding to the column and row of M_S. If all the elements in D_m are equal, the fault does not occur in this feeder. For the feeder with different elements in D_m, the fault cable can be located by

$$\begin{cases} \boldsymbol{\Gamma}_+ = \displaystyle\sum_{y \in \boldsymbol{\Phi}_+} M_S(i,y), \boldsymbol{\Gamma}_- = \displaystyle\sum_{y \in \boldsymbol{\Phi}_-} M_S(i,y) \\ V_F = sort\left(V_D(i) \right), N_{LF} = \left(\boldsymbol{\Theta}_+(V_F(1)), \boldsymbol{\Theta}_+(V_F(2)) \right), \boldsymbol{\Gamma}_+(i) = 2 \\ V_F = sort\left(V_D(i) \right), N_{LF} = \left(\boldsymbol{\Theta}_-(V_F(1)), \boldsymbol{\Theta}_-(V_F(2)) \right), \boldsymbol{\Gamma}_-(i) = 2 \end{cases} \quad (14)$$

where $\boldsymbol{\Phi}_+$ and $\boldsymbol{\Phi}_-$ represent the sets composed of the numbers of the MUs. The elements in $\boldsymbol{\Phi}_+$ and $\boldsymbol{\Phi}_-$ correspond to the positive and negative ones in D_m, respectively. $\boldsymbol{\Gamma}_+$ and $\boldsymbol{\Gamma}_-$ are

This article has been accepted for publication in a future issue of this journal, but has not been fully edited. Content may change prior to final publication. Citation information: DOI 10.1109/TPWRD.2022.3170294, IEEE Transactions on Power Delivery

> REPLACE THIS LINE WITH YOUR PAPER IDENTIFICATION NUMBER (DOUBLE-CLICK HERE TO EDIT) <　　　6

the vectors obtained by accumulating the elements in the rows of M_S corresponding to Φ_+ and Φ_-. Θ_+ and Θ_- denote the sets containing the nodes with the MUs in Φ_+ and Φ_-. The function *sort*( ) is used to find the elements (corresponding to Θ_+) in V_D and rearrange them in descending order. $\Theta_+(V_F(1))$ and $\Theta_-(V_F(1))$ represent the elements (corresponding to $V_F(1)$) in Θ_+ and Θ_-. N_{LF} contains the node information of the fault cable. It is written as the numbers of the nodes at both ends of the fault cable. It can be known from eq. (12) and eq. (14) that the direction instead of the phase angle of the grounding line current is used to locate the fault cable. Thus, strict synchronization is not required. The steps of the fault sensing algorithm implemented by the edge nodes are displayed below.

Algorithm: grounding line current based fault sensing
Input: Grounding line currents at local ends of the cables recorded by the MUs.
1.　Determine t_0, T and i_{LSM}.
2.　Number the network nodes and MUs.
3.　**If** criterion (5) is satisfied, **then**
4.　　**If** the network has an ungrounded neutral, **then**
5.　　　Compute D_m by (13) for each feeder.
6.　　　Find the D_m with different elements.
7.　　　Construct the corresponding M_S and V_D.
8.　　　Detect the fault cable by (14).
9.　　**Else**
10.　　　Filter the grounding line currents.
11.　　　Repeat steps 5-8.
12.　　**End**
13.　**Else** there is no fault occurs.
14.　**End**
Output: fault detection result or fault cable node N_{LF}.

III. PERFORMANCE EVALUATION

To validate the proposed algorithm, various faults are simulated in a typical 10kV distribution cable network model constructed by PSCAD/EMTDC. The diagram of the network is shown in Fig.6. The simulation models used in PSCAD/EMTDC are illustrated in Appendix *C*. is Switch K1 determines the neutral grounding mode of the network. CB1 and CB2 are the circuit breakers for connecting the three buses. CB3, CB4, and CB5 are the circuit breakers in the ring network cabinet. In normal operation, CB1 and CB2 are all closed while CB3, CB4, and CB5 are all disconnected. L1, L2, …, L24 represent the loads. All the cables are grounded at both terminals through the grounding lines. The sampling rate is set as 3.2 kHz. The grounding line current at the local end of each cable is measured. The resistance of the grounding line R_{SG} is 1Ω. EN1, EN2, and EN3 are the edge nodes receiving the measured grounding line currents and conducting the fault sensing algorithm. The type and parameter of the edge computing unit is listed in Table I. In the table, OS represents the operating system. PSV denotes the power source voltage. EN1 is located at the branch node (common connection mode) of cables 3, 4, and 5. EN2 is located at the branch node of cables 11, 12, and 13. EN3 is located at the branch node of cables 19, 20, and 21. The current data of all the cables fed by

Bus 1, 2, and 3 is transmitted to EN1, EN2, and EN3, respectively. Various faults simulations are conducted. The results are shown below.
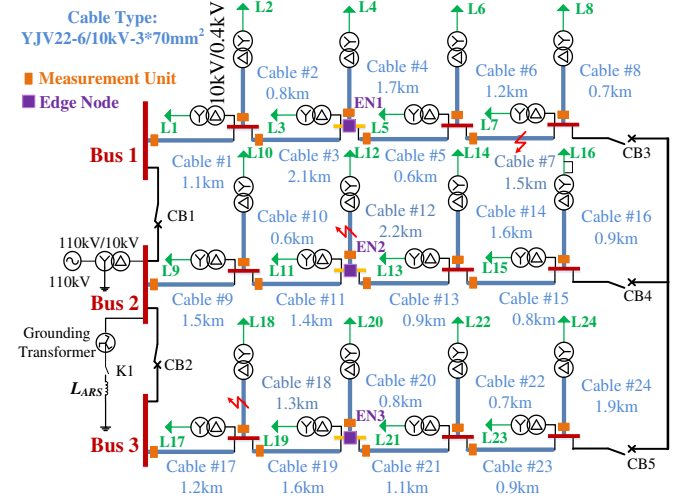

Fig.6 Diagram of the simulated distribution cable network.

Table I
TYPE AND PARAMETERS OF THE EDGE COMPUTING UNIT

Type	CPU and OS	RAM	ROM
EdgeBox-RPI	Broadcom BCM2837B0、Linux	1GB	32GB
	Interface	PSV	Size (mm)
	Ethernet/RS232/RS485/CAN-FD×2/USB×2/HDMI 4G/LTE	10.8V~36V	124×68×35

A. Case Study

Three different faults are simulated in this section. The details of the cases are shown in Table II. 'NGM' represents the neutral grounding mode of the network. 'UNG' and 'ASG' denote the ungrounded and arc-suppression coil grounded neutrals. 'x_F' represents the fault distance. R_{FS} is the fault resistance between the core conductor and the metallic sheath. R_{FG} is the fault resistance between the metallic sheath and the ground. θ_f is the fault resistance and inception angle.

Table II
DETAILS OF THE CASES

Case	NGM	Fault Cable	N_{LF}	R_{FS}	R_{FG}	θ_f	x_F
1	UNG	#7	N6,N8	10Ω	190Ω	30°	498m
2	ASG	#12	N4,N5	10Ω	10^6Ω	30°	1475m
3	UNG	#18	N2,N3	100Ω	400Ω	90°	721m

The grounding line currents at EN1, EN2, and EN3 in the three cases are depicted in Fig.7 and Fig.8. In the figures, the initial and filtered grounding line currents of cable #m ($1 \le m \le 24$) are denoted as i_{sm} and i_{smf} in the legends, respectively. It can be observed that the grounding line current varies significantly prior to and after the fault. The directions of the grounding line currents of the fault cable and those upstream the fault cable are identical. They are opposite to those of the remaining cables. The fault detection results are listed in Table III. In the table, 'FDR' represents the fault detection result. The currents in the columns EN1, EN2, and EN3 in the table are the maximum values of the ground line currents at EN1, EN2, and EN3. Since these currents are all far larger than i_{LSM}, the

cable faults can be correctly detected by the proposed criterion in (5). The nodes and MUs for the cable feeder are numbered and illustrated in Fig.9. N1, N2, …, N8 are the numbers of the nodes. M1, M2, …, M8 are the numbers of the MUs. Since the topologies of the three cable feeders are identical, these numbers are set to be the same values for the three feeders for convenience.
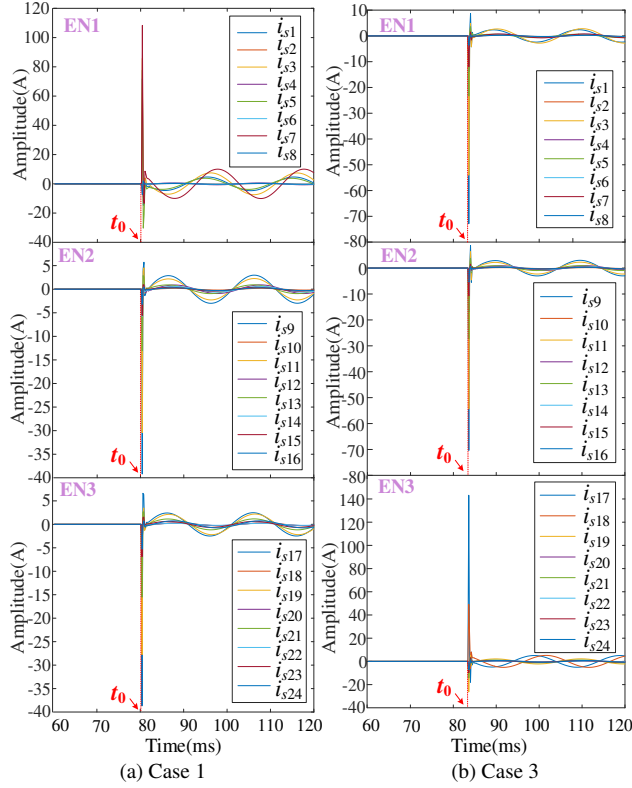

(a) Case 1   (b) Case 3

Fig.7 The grounding line currents at edge nodes in cases 1 and 3.
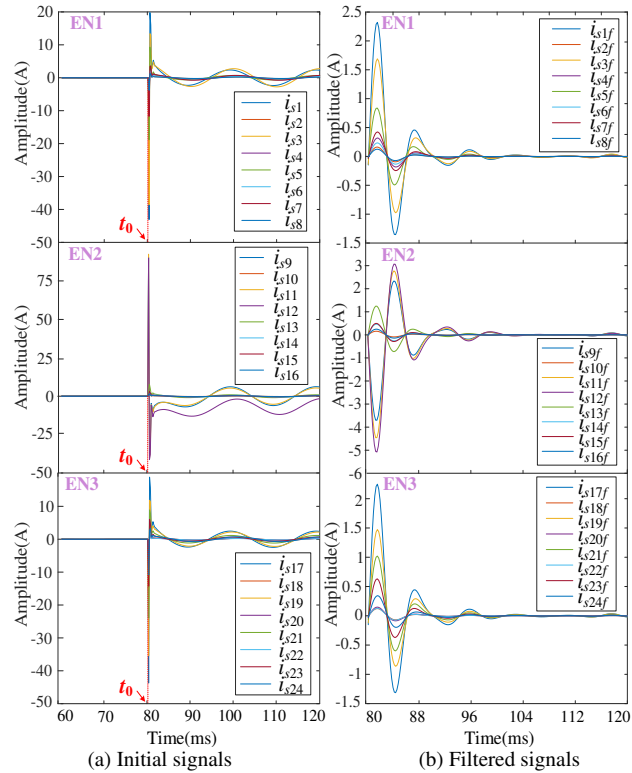

(a) Initial signals   (b) Filtered signals

Fig.8 The grounding line currents at edge nodes in case 2.

Table III
FAULT DETECTION RESULTS

Case	t_0	T	i_{LSM}	EN1	EN2	EN3	FDR
1	0.08s			2.76A	6.21A	2.46A	fault occurs
		0.02s	0.1A				
2	0.08s			10.04A	2.98A	2.48A	fault occurs

To locate the fault cable, the vectors of the direction factor (D_m) for the three cable feeders are computed at EN1, EN2, and EN3 in each case. The grounding line current of cable #1 is taken as a reference. The calculation results are listed in Table IV. To locate the fault cable section, the space matrix M_S and distance vector V_D corresponding to the feeders connected to Buses 1, 2, and 3 are created in cases 1, 2, and 3, respectively. The topologies of the three feeders are identical but the cable lengths are not, thus the space matrices in the three cases are equal but the distance vectors are not. M_S and V_D in the three cases are shown by (15)-(16). The fault cable section location results are listed in Table V. 'CN' represents the case number. Φ_+, Φ_-, Γ_+ (or Γ_-) and Θ_+ (or Θ_-) required in (14) are shown in the table. It can be clearly seen that the fault sections in the three cases can be correctly located by the proposed fault sensing algorithm.
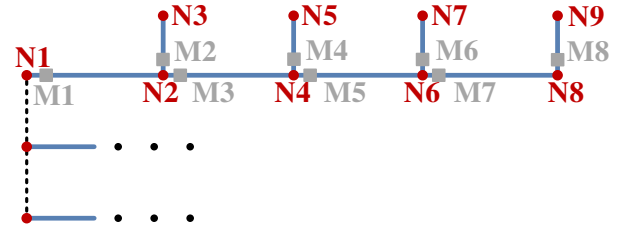

Fig.9 Numbers of the nodes and measurements in the network.

Table IV
VECTORS OF THE DIRECTION FACTOR IN THE THREE CASES

Case	D_m			Fault Feeder
	EN1	EN2	EN3	Feeder
1	**[1, -1,1,-1, 1,-1,1,-1]**	[-1,-1,-1,-1 ,-1,-1,-1,-1]	[-1,-1,-1,-1, -1,-1,-1,-1]	Connected to Bus 1
	EN1	EN2	EN3	Feeder
2	[1,1,1,1, 1,1,1,1]	**[-1,1,-1,- 1,1,1,1,1]**	[1,1,1,1, 1,1,1,1]	Connected to Bus 2
	EN1	EN2	EN3	Feeder
3	[1,1,1,1, 1,1,1,1]	[1,1,1,1, 1,1,1,1]	**[-1,-1,1,1, 1,1,1,1]**	Connected to Bus 3

$$M_S = \begin{bmatrix} - & M1 & M2 & M3 & M4 & M5 & M6 & M7 & M8 \\ N1 & 1 & 0 & 0 & 0 & 0 & 0 & 0 & 0 \\ N2 & 1 & 1 & 1 & 0 & 0 & 0 & 0 & 0 \\ N3 & 0 & 1 & 0 & 0 & 0 & 0 & 0 & 0 \\ N4 & 0 & 0 & 1 & 1 & 1 & 0 & 0 & 0 \\ N5 & 0 & 0 & 0 & 1 & 0 & 0 & 0 & 0 \\ N6 & 0 & 0 & 0 & 0 & 1 & 1 & 1 & 0 \\ N7 & 0 & 0 & 0 & 0 & 0 & 1 & 0 & 0 \\ N8 & 0 & 0 & 0 & 0 & 0 & 0 & 1 & 1 \\ N9 & 0 & 0 & 0 & 0 & 0 & 0 & 0 & 1 \end{bmatrix} \quad (15)$$

$$V_D = \begin{cases} \begin{bmatrix} 0 & 1.1 & 1.9 & 3.2 & 4.9 & 3.8 & 5 & 5.3 & 6 \end{bmatrix}^T, case\,1 \\ \begin{bmatrix} 0 & 1.5 & 2.1 & 2.9 & 5.1 & 3.8 & 5.4 & 4.6 & 5.5 \end{bmatrix}^T, case\,2 \\ \begin{bmatrix} 0 & 1.2 & 2.5 & 2.8 & 3.6 & 3.9 & 4.6 & 4.8 & 6.7 \end{bmatrix}^T, case\,3 \end{cases} \quad (16)$$

Table V
RESULTS OF FAULT CABLE SECTION LOCATION IN THE THREE CASES

CN	Φ_+	Φ_-	Γ	Θ	V_F	N_{LF}
1	M1,M3, M5,M7	M2,M4, M6,M8	$\Gamma_+(i)$ =2	N1,N2, N4,**N6**, **N8**	[**5.3**, **3.8**, 3.2,1.1,0]	N6,N8
2	M2,M5, M6,M7, M8	M1,M3, M4	$\Gamma_-(i)$ =2	N1,N2, **N4,N5**	[**5.1**,**2.9**,1.5 ,0]	N4,N5
3	M3,M4, M5,M6, M7,M8	M1,M2	$\Gamma_-(i)$ =2	N1,**N2**, **N3**	[**2.5**,**1.2**,0]	N2,N3

B. Sensitivity Analysis
1) Effects of Fault Conditions

To test the performance of the fault sensing algorithms in different fault conditions, the faults with various resistances, inception angles, and distances are simulated in different cable sections. The detailed information of the conducted simulations is listed in Table VI. 'FC' represents the number of the cable with faults. 'NF' denotes the total number of the simulated faults for each cable. Fig.10 displays the grounding line currents at the local ends of the fault cable #21 with different fault conditions. It can be observed that the fault resistances and inception angles mainly affect the amplitude value and variation of the grounding line current signal. The vectors of the direction factor for the cable feeder corresponding to the faults in cable #3 with different fault conditions are all identical. The direction factors for the faults in cables #3, #16, and #21 are depicted in Fig.11. The fault sensing results are shown in Table VII. 'Min(i_{LS})' represents the minimum amplitude of the grounding line current in different fault conditions. P_{FCL} denotes the accuracy of fault section location. From the results in Fig.11 and Table VII, it can be concluded that the proposed fault sensing algorithm is not affected by the fault conditions.

Table VI
INFORMATION OF THE SIMULATED FAULT CONDITIONS

FC	N_{LF}	NGM	$R_{FS}(\Omega)$	$R_{FG}(\Omega)$	θ_f (°)	x_F (m)	NF
#3	N2,N4				30,90	152,998, 2003	36
#16	N8,N9	ASG UNG	10,200	300, 500, 10^6	10,90	84,447, 811	36
#21	N4,N6				30,90	112,506, 1025	36

(a) Cable #3

(b) Cable #16

(c) Cable #21

Fig.11 Vectors of the direction factor of the faults in cables #3, #16, and #21.

Table VII
RESULTS OF FAULT SENSING IN DIFFERENT FAULT CONDITIONS

FC	i_{LSM}	Min(i_{LS})	FDR	Γ	Θ	P_{FCL}
#3		1.76A	fault occurs	$\Gamma_+(i)$=2	N1,**N2,N4**	100%
#16	0.1A	1.24A	fault occurs	$\Gamma_-(i)$=2	N1,N2,N4,N6,**N8,N9**	100%
#21		1.81A	fault occurs	$\Gamma_-(i)$=2	N1,N2,**N4,N6**	100%

2) Effects of Arcs

The arc is a special and worrisome fault case that commonly appears, for example, when the cable conductor makes an electrical contact with the poorly grounded objects [36]. To verify the sensitivity of the fault sensing algorithm to the arc faults, three arc fault cases with different fault locations are considered in simulation. The model in [37] is employed to simulate the arc fault. The model consists of two parts: a fixed impedance Z_f and a pair of antiparallel diodes. In the arc fault model, the fixed impedance Z_f is set as $(100+j0.314)$ Ω. The details of the fault cases are displayed in Table VIII. Fig.12 depicts the grounding line currents at EN1 and EN2 in case 1. It can be observed that the grounding line currents are distorted to a certain extent due to the arc. However, the direction features of the grounding line currents are not affected. The fault sensing results are listed in Table IX. 'FSR' represents the fault sensing result. The results in the table demonstrate that the fault sensing algorithm is not affected by the arcs.

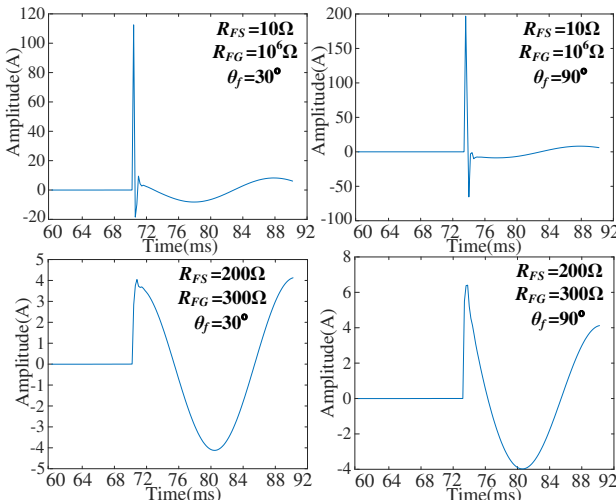

Fig.10 Grounding line currents in different fault conditions of cable #21.

Table VIII
DETAILS OF THE ARC FAULT CASES

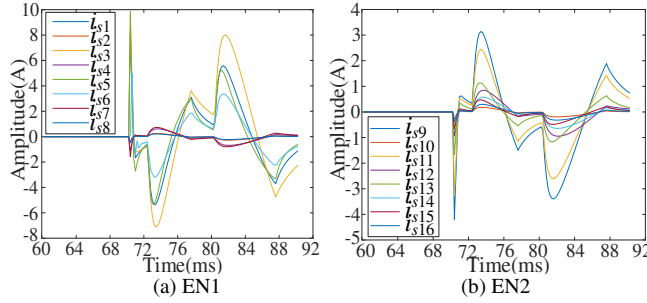| Case	FC	N_{LF}	NGM	x_F (m)
1	#6	N6,N7	UNG	517
2	#9	N1,N2	UNG	1294
3	#24	N8,N9	ASG	1663

Fig.12 Grounding line currents in cases 1.

Table IX
FAULT SENSING RESULTS OF THE ARC FAULT CASES

CN	Min(i_{LS})	FDR	Γ	Θ	FSR
1	2.94A	fault occurs	$\Gamma_+(i)=2$	N1,N2,N4,**N6,N7**	Correct
2	2.16A	fault occurs	$\Gamma_-(i)=2$	**N1,N2**	Correct
3	1.73A	fault occurs	$\Gamma_-(i)=2$	N1,N2,N4,N6,**N8, N9**	Correct

C. Discussions on the Presented Proposal of the MUs

Considering the actual installation conditions of the measurement units (MUs) in different distribution networks, it may be not feasible to mount the MU at every cable branch of a distribution network. In fact, for the proposed fault sensing algorithm, there also exists a better deployment proposal of the MUs. The details are explained as follows.

According to eq. (6), eq. (9) and eq. (11), it can be known that

$$\left|i_{js}(t)\right| = \sum_{\substack{k=1 \\ k \neq j}}^{M} \left|i_{ks}(t)\right| > \left|i_{ks}(t)\right|, \omega > \omega_C \quad (17)$$

In (17), operator '| |' is used to obtain the maximum of the signal. It can be observed that the grounding line current at the local end of the fault cable is larger than that of any healthy cable. Thus, for a branch node with M ($M>2$) cables, the relationship between the direction factors and maximum values of the grounding line currents at the local ends of these cables can be expressed by

$$\begin{cases} D_1 = D_2 = \cdots = D_{M-1}, \ case \ 1 \\ D_1 = D_2 = \cdots = D_{M-2} = -D_{M-1}, A_{M-1} > A_{M-2}, \ case \ 2 \end{cases} \quad (18)$$

where *case* 1 is that a fault occurs in a cable (the cable with Mth MU) without MU. *case* 2 means that a fault occurs in the cable with the $(M-1)$th MU. A_{M-1} and A_{M-2} represent the maximum values of the grounding line currents measured at the local end of the cables with the $(M-1)$th MU and $(M-2)$th MU. It can be known from eq. (18), the total number of the MUs for a branch node with M cables can be $M-1$, which has no effect on the fault sensing result.

For the case where there are only two cables ($M=2$) connected at the branch node and one cable (cable W) is located at the ending terminal of the fault feeder, if the fault

occurs in the cable at the ending terminal, the direction factors and maximum values of the grounding line currents of the cables in the fault feeder are

$$\begin{cases} D_1 = D_2 = \cdots = D_{W-1} = D_W \\ A_W > A_{W-1} \end{cases} \quad (19)$$

where W ($W>1$) is the total number of the cable branches in the fault feeder. If the fault occurs in another cable (cable $W-1$), the direction factors and maximum values of the grounding line currents of the cables in the fault feeder are

$$\begin{cases} D_1 = D_2 = \cdots = D_{W-1} = -D_W \\ A_{W-1} > A_W \end{cases} \quad (20)$$

It can be known from eq. (19) and eq. (20) that the fault cable cannot be located by using the direction factors and maximum values of the grounding line currents of the cables in the fault feeder if there is no MU at cable W.

In summary, the new deployment proposal of the MUs is as follows. First, for a branch node with M ($M>2$) cables, only $M-1$ cables must be equipped with the MUs. Then, if a branch node has only two cables and one cable is located at the ending terminal of the feeder, the MU must be installed at the local end of this cable. According to the proposal, the deployment of the MUs in Fig.6 is reshown in Fig.13. It can be observed that the MUs are not installed at every cable branch. The total number of the MUs decreased from 24 to 18, which further reduces the cost of the measurement system.

Based on the above measurement deployment proposal, the fault cable location method is simply extended as follows due to space limitation. It is assumed that there are K feeders and H_k cable branches for any feeder k ($1 \leq k \leq K$) (no MU is located at the local end of feeder k). First, the fault feeder is identified by

$$\begin{cases} N_{FD} = k, D_1 = D_2 = \cdots = D_{k-1} = D_{k+1} = \cdots = D_K \\ N_{FD} = K, D_1 = D_2 = \cdots = D_{k-1} = D_{k+1} = \cdots = -D_K \ and \ A_K > A_{k-1} \end{cases} \quad (21)$$

where N_{FD} represents the number of the fault feeder. It is assumed that the fault feeder has W cable branches with V MUs. If a MU is not located at the local end of the first cable, the fault cable(s) can be then located by

$$\begin{cases} N_{FC} = 1, D_1 = D_2 = \cdots = D_V \\ N_{FC} = V, A_V > A_{V-1}, \text{Ending terminal} \\ N_{FC} = \Phi_V, A_V > A_{V-1}, \text{Not ending terminal} \end{cases} \quad (22)$$

In (22), N_{FC} represents the number set of the fault cable(s). A_V and A_{V-1} represent the maximum values of the grounding line currents measured at the local end of the cables with the Vth MU and $(V-1)$th MU. Φ_V denotes the cables between the Vth MU and its adjacent MU in the feeder. If a MU is located the local end of the first cable, the fault cable(s) can be then located by

$$\begin{cases} N_{FC} = V, A_V > A_{V-1}, \text{Ending terminal} \\ N_{FC} = \Phi_V, A_V > A_{V-1}, \text{Not ending terminal} \end{cases} \quad (23)$$

To verify the extended method, the data in the fault case 1 in subsection III.A are employed. The calculation results of the above method are listed in Table X. D_F represents the

direction factor of the feeder. A_F denotes the maximum values of the grounding line currents measured at the local ends of the feeders. It can be observed that the fault cable can be correctly located by the extended method with the proposed measurement deployment.
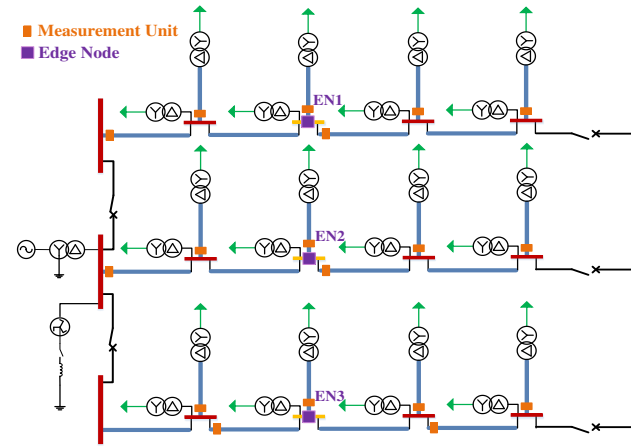

Fig.13 The new deployment of the MUs.

Table X
CALCULATION RESULTS OF THE EXTENDED METHOD BASED ON NEW MEASUREMENT DEPLOYMENT

CN	D_F	A_F	N_{FD}	$A_V > A_{V-1}$	N_{FC}
1	[1,-1]	[6.7A,3.2A]	1	$V=7$, $A_V=14.8A$	Cable#7
2	[-1,1]	[2.3A,3.5A]	2	$V=12$, $A_V=3.2A$	Cable#12
3	[1,1]	---	3	$V=18$, $A_V=8A$	Cable#18

D. Comparison Work
1) Comparison with Several Common Methods

A comparative study between the proposed fault sensing method and several common methods is conducted. The results are listed in Table XI. In the table, 'AGM' denotes the fault sensing algorithm. I_p and U_p represent the phase current and voltage signals. I_0, U_0 and I_S denote the zero-sequence current, zero-mode voltage and grounding line current signals. 'FD' represents the fault detection. Symbols '✓' and '×' represent if an additional criterion is required or not. 'DP' denotes the data processing system. 'SY' represents the time synchronization and 'PN' denotes the prior knowledge. 'R' and 'NR' represents if the item is required or not. f_S is the sampling rate and 'TC' denotes the three-core distribution cable. 'C' and 'NC' denote that the item is considered and not considered. All the comparison work is based on the same simulation test system shown in Fig.7. All the simulations are performed in a computer whose processor is Intel Core (TM) i5-6300HQ @ 2.3GHz.

Table XI
COMPARISON RESULTS WITH SEVERAL METHODS

AGM	Signal	FD	DP	SY	PN	f_S	TC	Arc
[12]	I_P	✓	CDS	R	R	25kHz	NC	NC
[15]	U_p	✓	CDS	R	R	5kHz	NC	NC
[20]	I_p, I_0	×	CDS	R	R	7.68kHz	NC	NC
[37]	U_0	×	CDS	NR	R	50kHz	NC	C
Proposed algorithm	I_S	×	ECS	NR	NR	3.2kHz	C	C

The methods in [12], [15], and [20] can be directly used to

locate the fault cable. The method in [37] uses the amplitude ratio of the transient zero-sequence voltages measured at both ends of each distribution line to identify the fault feeder. However, it should be noted that it can be also used to locate the fault cable by applying the method to each branch node. The detailed implementation steps are as follows. First, the fault feeder is determined by the method in [37]. In the fault feeder, there are many branch nodes of the distribution lines. Then, for each branch node, the fault line is identified by reusing the method. Finally, the actual fault line section is determined by comparing the determination results at the branch nodes. In the comparison work, the method in [37] is employed to locate the fault cable by following the above steps. The calculation results show that the fault cable can be located by the method in [37].

From the results in Table XI, it can be seen that the phase voltages, currents, or zero-sequence components are used in the methods in [12], [15], [20] and [37]. The methods in [12] and [15] require additional criteria for fault detection while the method in [20] does not. The methods in [12], [15], and [20] adopt the CDS, require strict time synchronization, and need the prior knowledge. The arc faults and three-core cables are not considered in the three methods. Since the amplitude of the transient zero-sequence voltage is used in [37], the fault detection and strict synchronization are not required. As a transient method, the method in [37] is also applicable to the arc faults. However, it is not easy to acquire the voltages (needed in the method) at both ends of the distribution cable for centralized data processing due to the difficulty of installing the voltage transformers. The voltage information of the bus fault (prior knowledge) is required in [37] before locating the fault section. Since the transient frequency components are extracted in the method, high sampling rate (up to 50kHz) is necessary in [37]. In addition, the method in [37] does not consider the structure and parameters of the distribution cable.

Compared with these methods, the proposed method only uses the grounding line currents. They have larger amplitudes than the zero-sequence currents, which has been proved by both theoretical analysis (in Appendix *B*) and simulation results (in Fig.5). As explained in section II. *B*, it is easier to measure the grounding line currents than the zero-sequence ones. Since only the direction information of the grounding line currents is employed for both ordinary and arc faults, strict synchronization and prior knowledge are not required. The method requires the lowest sampling rate (only 3.2 kHz). It also considers the three-core cable. In general, the proposed algorithm has more advantages.

2) Comparison with the Method in Ref. [38]

The reference [38] also uses the sheath current of the cable. However, there exist significant differences between the method in reference [38] and the proposed one.

First, the research objects in the reference and this paper are totally different. Although the cable systems are involved in the reference and this paper, voltage rates, structures and parameters of the cables in the two papers are totally different. The type of the cable in the reference is cross-bonded single-

This article has been accepted for publication in a future issue of this journal, but has not been fully edited. Content may change prior to final publication. Citation information: DOI 10.1109/TPWRD.2022.3170294, IEEE Transactions on Power Delivery

> REPLACE THIS LINE WITH YOUR PAPER IDENTIFICATION NUMBER (DOUBLE-CLICK HERE TO EDIT) <   11

core cable while that in this paper is three-core cable. The voltage rate of the cable in the reference is 110kV while that in this paper is only 10kV. Thus, the electrical parameters (impedance and admittance matrices) of the cables in the two papers are also different. As shown in Fig.14, the three-core cable in this paper requires double-end grounding, only one grounding line current at the local end is acquired by the measurement unit (MU) in every cable. The single-core cable in the reference requires single-end sectionalized cross-bonded grounding. For each cable, at least three-phase grounding line currents are sampled by three MUs.
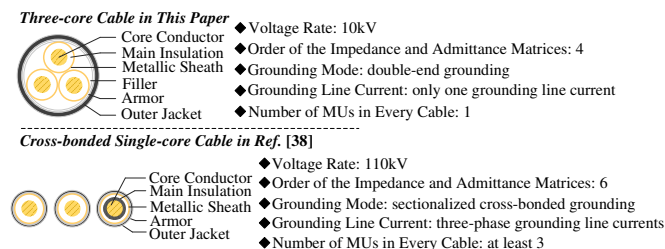

Fig.14 Differences between the research objects in reference [38] and this paper.

Second, the model and analysis method in the reference and this paper have nothing in common. In the reference, the single-core cable is modelled as a two-port network in phase domain. The steady-state analysis method is then used. However, in this paper, the three-core cable is modelled as a lump-parameter equivalent circuit in time domain composed of the impedances and admittances of the core-conductors and metallic sheath. The transient-state analysis is employed.

Third, the fault sensing algorithms in the reference and this paper are distinct. In the reference, the fault sensing algorithm is summarized by the conclusion of the simulation analysis, thus no specific theoretical analysis is conducted. The phase angle differences between the sheath currents in fundamental frequency of the neighboring cable sections are used to locate the fault cable. The algorithm only aims at one cable line, thus it is not applicable to the distribution network with feeders and branches. The algorithm in the reference requires strict synchronization to obtain the accurate phase angles of the three-phase sheath currents. Since the steady-state sheath currents are used, the algorithm is not applicable to the arc faults. However, in this paper, the fault sensing algorithm is developed based on rigorous theoretical analysis and validated by various fault simulations. The direction factors and amplitudes of the sampled grounding line currents in the time domain are utilized to detect the cable fault and locate the fault cable. Thus, the proposed algorithm can be applied to the arc faults and strict synchronization is not necessary. The proposed algorithm is applicable to the actual distribution network with many feeders and branches.

IV. Conclusions

Aiming at the power distribution cable network, this paper presents a novel algorithm implemented at the edge nodes to sense the fault. The edge nodes only employ the grounding line current at the local end of the cable, which realizes fast and reliable fault sensing. General conclusions are as follows.

First, the grounding line current at the local end of a distribution cable can be expressed by an exponential decay function, whose value is close to zero in normal operation.

Second, after a fault occurs in the cable network, the grounding line current of each cable increases significantly. It is verified to be related to the zero-sequence current in theory. The relationship can be expressed by a differential equation of first order based on the cable model. Additionally, the amplitude of the grounding line current is larger than that of the zero-sequence current at the local end of the cable in the same fault condition, making it more appropriate to use the grounding line current to sense the cable fault.

Third, the directions of the grounding line currents of the fault cable feeder are opposite to those of the healthy feeders. Combining the distribution network topology, locations of the MUs and direction information of the grounding line current, the fault cable section can be located by the proposed space matrix based algorithm in the edge nodes.

The future work mainly includes the verification of the proposed method by using the measured data from a real distribution cable network.

References

[1] H. Shu, X. Liu and X. Tian, "Single-ended fault location for hybrid feeders based on characteristic distribution of traveling wave along a line," *IEEE Transactions on Power Delivery*, vol. 36, no. 1, pp. 339-350, Feb. 2021.

[2] M. Guo, J. Gao, X. Shao and D. Chen, "Location of single-line-to-ground fault using 1-D convolutional neural network and waveform concatenation in resonant grounding distribution Systems," *IEEE Transactions on Instrumentation and Measurement*, vol. 70, pp. 1-9, 2021.

[3] M. Kazim, A. H. Khawaja, U. Zabit and Q. Huang, "Fault detection and localization for overhead 11-kV distribution lines with magnetic measurements," *IEEE Transactions on Instrumentation and Measurement*, vol. 69, no. 5, pp. 2028-2038, May 2020.

[4] Y. Xue, X. Chen, H. Song and B. Xu, "Resonance analysis and faulty feeder identification of high-impedance faults in a resonant grounding system," *IEEE Transactions on Power Delivery*, vol. 32, no. 3, pp. 1545-1555, June 2017.

[5] X. Zeng, K. Yu, Y. Wang and Y. Xu, "A novel single phase grounding fault protection scheme without threshold setting for neutral ineffectively earthed power systems," *CSEE Journal of Power and Energy Systems*, vol. 2, no. 3, pp. 73-81, Sept. 2016.

[6] M. A. Barik, A. Gargoom, M. A. Mahmud, M. E. Haque, H. Al-Khalidi and A. M. Than Oo, "A decentralized fault detection technique for detecting single phase to ground faults in power distribution systems with resonant grounding," *IEEE Transactions on Power Delivery*, vol. 33, no. 5, pp. 2462-2473, Oct. 2018.

[7] C. Gonzalez, J. Tant, J. G. Germain, T. De Rybel and J. Driesen, "Directional, high-impedance fault detection in isolated neutral distribution grids," *IEEE Transactions on Power Delivery*, vol. 33, no. 5, pp. 2474-2483, Oct. 2018.

[8] W. Zhang, X. Xiao, K. Zhou, W. Xu and Y. Jing, "Multicycle incipient fault detection and location for medium voltage underground cable," *IEEE Transactions on Power Delivery*, vol. 32, no. 3, pp. 1450-1459, June 2017.

[9] M. A. Shokry, A. Khamlichi, F. Garnacho, J. M. Malo and F. Álvarez, "Detection and localization of defects in cable sheath of cross-bonding configuration by sheath currents," *IEEE Transactions on Power Delivery*, vol. 34, no. 4, pp. 1401-1411, Aug. 2019.

[10] D. Xiao, T. He, R. Xiao, X. Du, "Segment location for single-phase-to-ground fault in neutral non-effectively grounded system based on distributed electric-field measurement," *Electric Power Systems Research*, vol. 184, 2020.

[11] A. A. P. Bíscaro, R. A. F. Pereira, M. Kezunovic, and J. R. S. Mantovani, "Integrated fault location and power-quality analysis in electric power distribution systems," *IEEE Transactions on Power Delivery*, vol. 31,

This article has been accepted for publication in a future issue of this journal, but has not been fully edited. Content may change prior to final publication. Citation information: DOI 10.1109/TPWRD.2022.3170294, IEEE Transactions on Power Delivery

> REPLACE THIS LINE WITH YOUR PAPER IDENTIFICATION NUMBER (DOUBLE-CLICK HERE TO EDIT) <   12

no. 2, pp. 428–436, Apr. 2016.

[12] M. Daisy and R. Dashti, "Single phase fault location in electrical distribution feeder using hybrid method," *Energy*, vol. 103, pp. 356-368, Feb. 2016.

[13] K. Jia, Z. Ren, T. Bi and Q. Yang, "Ground fault location using the low-voltage-side recorded data in distribution systems," *IEEE Transactions on Industry Applications*, vol. 51, no. 6, pp. 4994-5001, Nov.-Dec. 2015.

[14] X. Dong, J. Wang, S. Shi, B. Wang, B. Dominik and M. Redefern, "Traveling wave based single-phase-to-ground protection method for power distribution system," *CSEE Journal of Power and Energy Systems*, vol. 1, no. 2, pp. 75-82, June 2015.

[15] R. Dashti and J. Sadeh, "Fault section estimation in power distribution network using impedance-based fault distance calculation and frequency spectrum analysis," *IET Generation, Transmission & Distribution*, vol. 8, no. 8, pp. 1406-1417, Jan. 2014.

[16] W. C. Santos, F. V. Lopes, N. S. D. Brito, and B. A. Souza, "High impedance fault identification on distribution networks," *IEEE Transactions on Power Delivery*, vol. 32, no. 1, pp. 23–32, Feb. 2017.

[17] X. Wang, J. Gao , M. Chen, X. Wei, Y. Wei, and Z. Zeng, "Faulty line detection method based on optimized bistable system for distribution network," *IEEE Transactions on Industrial Informatics*, vol. 14, no. 4, pp. 1370-1381, Apr. 2018.

[18] T. Jin and H. Li, "Fault location method for distribution lines with distributed generators based on a novel hybrid BPSOGA," *IET Generation, Transmission & Distribution*, vol. 10, no. 10, pp. 2454-2463, Jul. 2016.

[19] X. Wang, H. Zhang, F. Shi, Q. Wu, V. Terzija, W. Xie, and C. Fang, "Location of single phase to ground faults in distribution networks based on synchronous transients energy analysis," *IEEE Transactions on Smart Grid*, vol. 11, no. 1, pp. 774-785, Jan. 2020.

[20] A. C. Adewole, R. Tzoneva, and S. Behardien, "Distribution network fault section identification and fault location using wavelet entropy and neural networks," *Applied Soft Computing*, vol. 46, pp. 296-306, May 2016.

[21] Y. Xi, Z. Li, X. Zeng, X. Tang, X. Zhang, H. Xiao, "Fault location based on travelling wave identification using an adaptive extended Kalman filter," *IET Generation, Transmission & Distribution*, vol. 31, pp. 1314-1322, Feb. 2018.

[22] L. Xie, L. Luo, Y. Li, Y. Zhang and Y. Cao, "A traveling wave-based fault location method employing VMD-TEO for distribution network," *IEEE Transactions on Power Delivery*, vol. 12, no. 4, pp. 1987-1998, Aug. 2020.

[23] X. Chen, X. Yin, and S. Deng, "A novel method for slg fault location in power distribution system using time lag of travelling wave components," *IEEJ Transactions on Electrical & Electronic Engineering*, vol. 12, pp. 45-54, Nov. 2016.

[24] Z. He, X. Liu, X. Li and R. Mai, "A novel traveling-wave directional relay based on apparent surge impedance," *IEEE Transactions on Power Delivery*, vol. 30, no. 3, pp. 1153-1161, June 2015.

[25] K. Jia, B. Yang, X. Dong, T. Feng, T. Bi and D. W. P. Thomas, "Sparse voltage measurement-based fault location using intelligent electronic devices," *IEEE Transactions on Smart Grid*, vol. 11, no. 1, pp. 48-60, Jan. 2020.

[26] K. Sun, Q. Chen, and Z. Gao, "An automatic faulted line section location method for electric power distribution systems based on multi-source information," *IEEE Transactions on Power Delivery*, vol. 31, no. 4, pp. 1542-1551, Aug. 2015.

[27] D. S. Kumar, S. J S. and B. S S., "Micro-synchrophasor based special protection scheme for distribution system automation in a smart city," *Protection and Control of Modern Power Systems*, vol. 5, no. 1, pp. 97-110, 2020.

[28] J. Teng, W. Huang and S. Luan, "Automatic and fast faulted line-section location method for distribution systems based on fault indicators," *IEEE Transactions on Power Systems*, vol. 29, no. 4, pp. 1653-1662, July 2014.

[29] I. Kiaei, and S. Lotfifard, "Fault section identification in smart distribution systems using multi-source data based on fuzzy petri nets," *IEEE Transactions on Smart Grid*, vol. 11, no. 1, pp. 74-83, Jan. 2020.

[30] J. Pan and J. McElhannon, "Future edge cloud and edge computing for internet of things applications," *IEEE Internet of Things Journal*, vol. 5, no. 1, pp. 439-449, Feb. 2018.

[31] N. Abbas, Y. Zhang, A. Taherkordi, and T. Skeie, "Mobile edge computing: a survey," *IEEE Internet of Things Journal*, vol. 5, no. 1, pp. 450-465, Feb. 2018.

[32] W. Shi, J. Cao, Q. Zhang, Y. Li, and L. Xu, "Edge computing: vision

and challenges," *IEEE Internet of Things Journal*, vol. 3, no. 5, pp. 637-646, Oct. 2016.

[33] C. Chen, Y. Chen, K. Zhang, M. Ni, S. Wang and R. Liang, "System redundancy enhancement of secondary frequency control under latency attacks," *IEEE Transactions on Smart Grid*, vol. 12, no. 1, pp. 647-658, Jan. 2021.

[34] Y. Li, L. Wu, P. Wouters, P. Wagenaars, P. V. D. Wielen and E. Steennis. "Effect of ground return path on partial discharge signal propagation along single-core and three-core power cables," *International Transactions on Electrical Energy Systems* 26 (2016): 1783-1798.

[35] M. Guo and N. Yang, "Features-clustering-based earth fault detection using singular-value decomposition and fuzzy c-means in resonant grounding distribution systems," *International Journal of Electrical Power & Energy Systems*, vol. 93,pp. 97–108, Dec. 2017.

[36] R. G. Ferraz, L. U. Iurinic, and A. D. Filomena, "Arc fault location: A nonlinear time varying fault model and frequency domain parameter estimation approach," *International Journal of Electrical Power & Energy Systems*, vol. 80, pp. 347–355, Sep. 2016.

[37] N. Peng, K. Ye, R. Liang, et al., "Single-phase-to-earth faulty feeder detection in power distribution network based on amplitude ratio of zero-mode transients," *IEEE Access*, vol. 7, pp. 117678-117691, 2019.

[38] Mingzhen Li, Wenjun Zhou, Chunlin Wang, et al., "A novel fault localization method based on monitoring of sheath current in a cross-bonded HV cable system," 2017 IEEE Electrical Insulation Conference (EIC), 2017, pp. 123-126.

APPENDIX

A. *Electrical Model of the Distribution Three-core Cable*

The electrical model of the cable in normal operation is shown in Fig.A1. l is the total length of the cable. R_{SG} represents the resistance of the grounding line. Z_{LP} denotes the equivalent impedance of the load in phase P. When a single-phase fault occurs in the cable, the electrical model of the fault cable is depicted in Fig.A2. R_{FS} and R_{FG} are the fault resistances. The fault distance is represented by x.
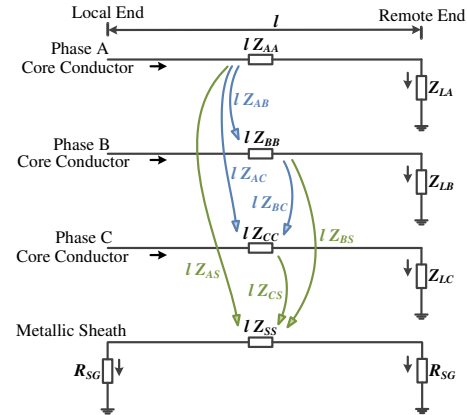

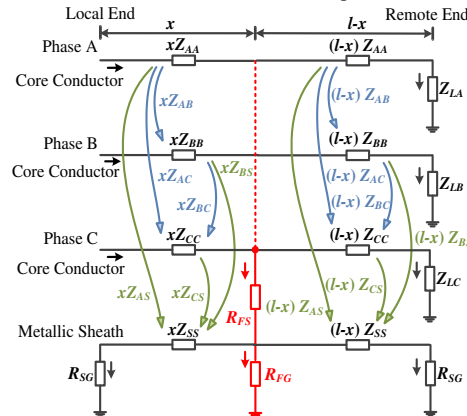Fig.A1 Model of the distribution cable in normal operation.

Fig.A2 Model of the distribution cable with a single-phase fault.

This article has been accepted for publication in a future issue of this journal, but has not been fully edited. Content may change prior to final publication. Citation information: DOI 10.1109/TPWRD.2022.3170294, IEEE Transactions on Power Delivery

> REPLACE THIS LINE WITH YOUR PAPER IDENTIFICATION NUMBER (DOUBLE-CLICK HERE TO EDIT) <   13

B. Theoretical Analysis of the Relationship between the Grounding Line Currents and Zero-sequence Ones

After the fault occurs, the zero-sequence current $i_{0k}(t)$ of cable k can be represented by $i_{0k}(t)=A\cos(\omega t+\varphi)$ where A, ω and φ represent the amplitude, angular frequency and initial phase of the current, respectively. According to (6),

$$h_k i_{ks}(t) + g_k \frac{di_{ks}(t)}{dt} = n_k i_{0k}(t) + w_k \frac{di_{0k}(t)}{dt} \tag{B1}$$
$$= A_k \cos(\omega t + \varphi) - B_k \sin(\omega t + \varphi)$$

In (B1), $A_k=n_k A$ and $B_k=\omega w_k A$. By rearranging (B1), we have

$$\frac{di_{ks}(t)}{dt} + \frac{h_k}{g_k} i_{ks}(t) = \frac{A_k}{g_k}\cos(\omega t + \varphi) - \frac{B_k}{g_k}\sin(\omega t + \varphi) \tag{B2}$$

Solving (B2), the grounding line current at the local end of cable k after the fault is expressed by

$$i_{ks}(t) = e^{-\int \frac{h_k}{g_k}dt}\left[\int\left(\frac{A_k}{g_k}\cos(\omega t + \varphi) - \frac{B_k}{g_k}\sin(\omega t + \varphi)\right)e^{\int \frac{h_k}{g_k}dt}dt + C\right] \tag{B3}$$

$$\begin{cases}\int\cos(\omega t+\varphi)\cdot e^{\frac{h_k}{g_k}t}dt = \dfrac{h_k g_k\cos(\omega t+\varphi)\cdot e^{\frac{h_k}{g_k}t} + g_k^2\omega\sin(\omega t+\varphi)\cdot e^{\frac{h_k}{g_k}t}}{h_k^2 - g_k^2\omega^2} \\[2mm] \int\sin(\omega t+\varphi)\cdot e^{\frac{h_k}{g_k}t}dt = \dfrac{h_k g_k\sin(\omega t+\varphi)\cdot e^{\frac{h_k}{g_k}t} - g_k^2\omega\cos(\omega t+\varphi)\cdot e^{\frac{h_k}{g_k}t}}{h_k^2 + g_k^2\omega^2}\end{cases} \tag{B4}$$

In (B3), C is a constant. By substituting (B4) into (B3), $i_{ks}(t)$ can be formulated by

$$\begin{cases}i_{ks}(t) = a\sin(\omega t + \varphi) + b\cos(\omega t + \varphi) + C \\ \qquad = \sqrt{a^2 + b^2}\sin(\omega t + \varphi + \theta) + C \\[2mm] a = \dfrac{A_k g_k\omega}{h_k^2 - g_k^2\omega^2} - \dfrac{B_k h_k}{h_k^2 + g_k^2\omega^2} \\[2mm] b = \dfrac{A_k h_k}{h_k^2 - g_k^2\omega^2} + \dfrac{B_k g_k\omega}{h_k^2 + g_k^2\omega^2} \\[2mm] \theta = \arctan\left(\dfrac{b}{a}\right)\end{cases} \tag{B5}$$

Therefore, the amplitude of $i_{ks}(t)$ is

$$\sqrt{a^2 + b^2} = A\sqrt{\frac{n_k^2\left(h_k^2 + g_k^2\omega^2\right)}{\left(h_k^2 - g_k^2\omega^2\right)^2} + \frac{w_k^2\omega^2}{h_k^2 + g_k^2\omega^2}} \tag{B6}$$

For the distribution cable, $R_{SG}=1\Omega$, $l_k=1$km, $L_{PS}=4.185\times10^{-6}$H. By calculation, the amplitude of $i_{ks}(t)$ is about 1.732A, which is larger than that of $i_{0k}(t)$.

C. Simulation Models used in PSCAD/EMTDC

The models in the simulation include the distribution cable model, transformer model, and load model. The three-phase two-winding transformer and the three-phase load models are depicted in Fig.A3. For the distribution cable, the frequency dependent (phase) model of the three-core pipe cable which effectively reflects the frequency variation features of the impedance and admittance parameters is employed in simulation. Fig.A4 shows the distribution cable model.
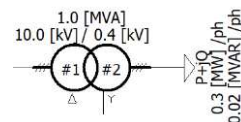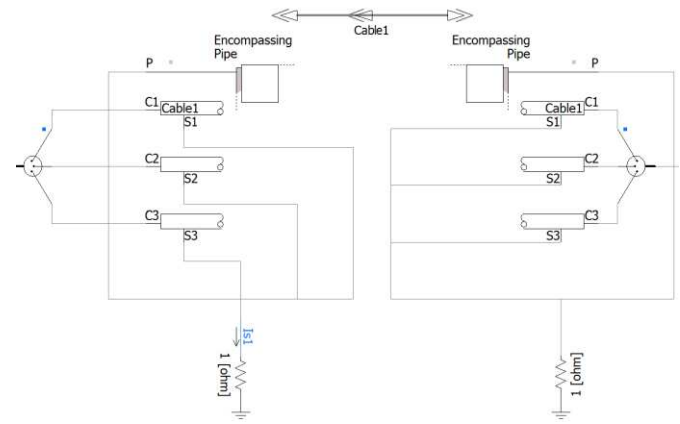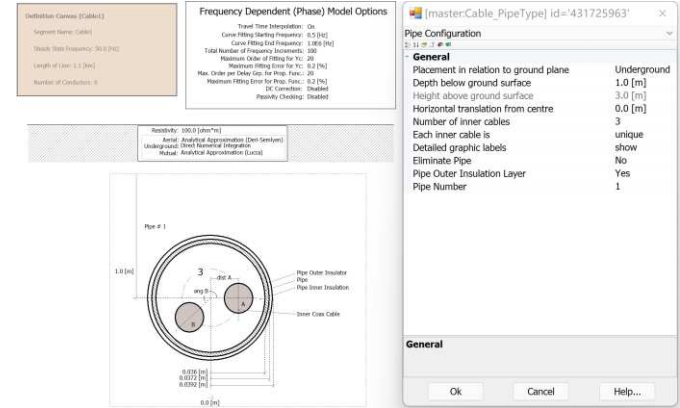
Fig.A3 The transformer and load models in PSCAD/EMTDC.

(a) Three-core pipe cable model in upper layer.

(b) Three-core pipe cable model in sublayer.
Fig. A4 Simulation model of the distribution cable in PSCAD/EMTDC.